Editors' Suggestion

Observation of Bistable Turbulence in Quasi-Two-Dimensional Superflow

E. Varga,* V. Vadakkumbatt, A. J. Shook, P. H. Kim, and J. P. Davis†
Department of Physics, University of Alberta, Edmonton, Alberta T6G 2E1, Canada

(Received 14 February 2020; revised 15 April 2020; accepted 2 June 2020; published 7 July 2020)

Turbulent flow restricted to two dimensions can spontaneously develop order on large scales, defying entropy expectations and in sharp contrast with turbulence in three dimensions where nonlinear turbulent processes act to destroy large-scale order. In this work we report the observation of unusual turbulent behavior in steady-state flow of superfluid ^{4}He—a liquid with vanishing viscosity and discrete vorticity—in a nearly two-dimensional channel. Surprisingly, for a range of experimental parameters, turbulence is observed to exist in two bistable states. This bistability can be well explained by the appearance of large-scale regions of flow of opposite vorticity.

DOI: 10.1103/PhysRevLett.125.025301

Chaotic motion of flowing fluids—turbulence—is one of the most ubiquitous phenomena occurring in nature and is frequently encountered in everyday life. Typically, the turbulence that one encounters takes place in three dimensions (3D); however, two-dimensional (2D) turbulence, while not perfectly realized in nature, is relevant to systems where motion in two dimensions dominates over the third, such as large-scale flows in oceans [1], atmospheres [2], soap bubbles [3], or liquid crystal films [4]. The hallmark feature of turbulence in three dimensions is the transfer of energy from large scales to small scales in both classical [5] and quantum [6] fluids. This "Kolmogorov cascade" can be understood as the splitting of large eddies in the flow into progressively smaller ones, until viscous damping dominates and dissipates the kinetic energy of small scales into heat. Turbulence in 3D therefore acts to destroy any large-scale ordering and, indeed, homogeneous and isotropic turbulence is an excellent approximation in many cases.

Restricting the flow of a classical fluid to 2D disrupts this homogenizing behavior. Interestingly, the direction of the cascade of energy can be inversed [7,8] and vorticity can coalesce into large eddies, thus spontaneously generating large-scale order from forcing on smaller scales. If the vorticity of the system is discrete (e.g., the quantized vortices in Bose-Einstein condensates [9,10] or the superfluid phases of ^{3}He and ^{4}He [11], as opposed to continuous vorticity of classical fluids), one can treat the system as a "gas" of pointlike vortices, which can be analyzed using the tools of statistical mechanics. In his pioneering work, Onsager [12] showed that such a gas can exist at effectively negative temperatures, which would physically manifest as clusters of like-signed vortices (i.e., configurations with high energy and low entropy), similar to the large-scale eddies in 2D classical fluids.

Sixty years after its prediction, the Onsager vortex gas has recently been observed, first using quantized vortices in Bose-Einstein condensates (BECs) [9,10] and then using a nanometer-thick film of superfluid ^{4}He [11]. These systems, however, contained only a small number of vortices ($N < 50$) and were allowed to decay freely during the experiment. Therefore, open questions remain as to the robustness of this phenomenon in macroscopic systems with large number of vortices and in steady-state flows (regimes approached so far only in simulations [13,14]). In this work, we study a forced and strongly turbulent oscillatory flow in a micrometer-thick slab of superfluid ^{4}He with macroscopic (millimeter-scale) lateral size. Turbulence in this system can exist in two nearly degenerate bistable states, both different from the laminar (i.e., nonturbulent) state. The transitions between these individual flow states are discontinuous, hysteretic, and a highly unusual "backward" transition from a less-turbulent to more-turbulent state upon decrease in velocity is observed. We argue that these observations stem from quasi-2D physics and that both the bistability and backward transition are naturally explained in terms of spontaneous flow polarization, suggesting the presence of large-scale order.

We study turbulence in superfluid ^{4}He (He II), which behaves as a mixture of two distinct fluid components [15]—an inviscid superfluid, where vorticity is restricted to discrete quantized vortices, and a normal fluid, with continuous vorticity and finite viscosity. He II has proven to be a valuable test bed [16–19] for the study of turbulence with both continuous and discrete vorticity, as well as the interactions between them.

Here, oscillatory flow is excited inside a microfluidic Helmholtz resonator [20–22] immersed in He II, where flow is limited to nearly two dimensions by confinement in the vertical direction [$D = 1067$ nm, Fig. 1(a)]. A uniform confinement, while somewhat larger than the thickness of previously used adsorbed films [11], avoids dissipative effects stemming from vortex-surface interactions [23]. Because of this strong confinement, only the superfluid component of He II can move (the normal component being

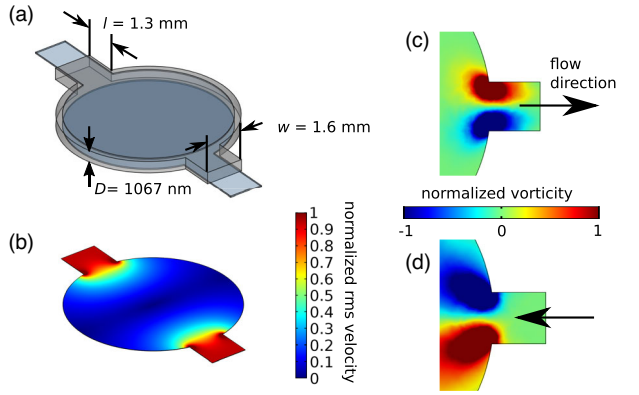

FIG. 1. Polarized vorticity in a 2D Helmholtz resonator. (a) Sketch of the device. The central circular basin, which is only used to drive and sense the flow, is connected to the surrounding bath of He II through two side channels. (b) Simulation of the Helmholtz mechanical mode, showing the normalized root-mean-square velocity concentrated in the channels. (c), (d) Vorticity is induced by sharp corners during the forward and reverse stroke of the mechanical mode; arrow indicates the superfluid flow direction. The positive and negative vortices are well separated in space [cf. the vortex generation terms $g_{\pm}$ in Eqs. (1) and (2)] and the injection of vorticity into the channel is thus strongly polarized [cf. the vortex polarization generation term g_s in Eq. (4)].

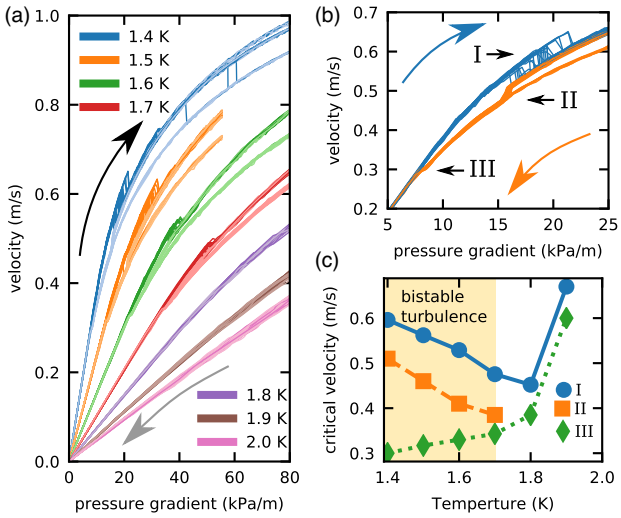

FIG. 2. Bistable turbulence and critical velocities. (a) The measured flow velocity as a function of applied pressure gradient for a range of temperatures. Darker curves show increasing pressure gradient, lighter decreasing (as indicated by the curved arrows). (b) Detail of the laminar-to-turbulent transition at 1.4 K. Blue curves correspond to increasing drive, orange to decreasing drive. Three critical velocities with discontinuous jumps are apparent: I, transition from laminar to turbulent state upon increasing velocity; II, the unusual backward transition into a more dissipative state upon decrease in velocity; III, transition from turbulent state back to laminar flow. Above I, the flow can randomly transition into the more dissipative state (not shown; see Ref. [24]). (c) The temperature dependence of the critical velocities of the three types labeled in (b). Onset of the bistable turbulence coincides with the appearance of the critical velocity II of the backward transition.

viscously clamped [21]). The resonator is microfabricated from single-crystal quartz and consists of a central circular basin connected to a surrounding bath of He II through two equal opposing channels of rectangular cross section [Fig. 1(a)]. The capacitive driving and sensing of the flow (see Refs. [20–22,24] for more details) allows us to measure the relationship between the driving pressure gradient and the fluid velocity in the channel of the resonator. The confinement used in this study was 1067 nm, but qualitatively similar results were also obtained for 805 nm confinement (see Ref. [24]).

A simulation of the fluid Helmholtz mechanical mode, Fig. 1(b), shows that the flow velocity is essentially confined to the two side channels. As the fluid flows into or out of the channel, the sharp corners at the channel end induce a vorticity in the flow, as seen in Figs. 1(c) and 1(d). On the forward stroke [fluid flowing into the channel, Fig. 1(c)] vorticity is injected into the channel in a polarized fashion. On the reverse stroke [Fig. 1(d)] vorticity is ejected and lost into the basin. The two side channels are identical; thus any flow instabilities are likely to occur approximately simultaneously.

To study the dissipation in this quasi-2D flow we resonantly drive the Helmholtz mechanical mode and continuously increase or decrease the drive amplitude (no significant dependence on ramp rate was observed). Several repeated measurements of peak velocity as a function of peak applied pressure at nominally identical conditions are shown in Figs. 2(a) and 2(b). For small drives the behavior is linear (i.e., the flow is laminar). With increasing drive, however, the measured velocity falls short of the value expected by extrapolating from the linear regime. That is, above a critical velocity the flow is damped by a drag with nonlinear dependence on velocity. The damping in the linear regime is believed to be dominated by the thermoviscous effect [21], whereas the nonlinear damping is predominantly due to the presence of quantized vortices [37]. The transition to the nonlinear regime is hysteretic and is marked by a discontinuous jump in the velocity-pressure dependence. For temperatures below 1.7 K, the velocity-pressure dependence in the nonlinear regime randomly follows one of two distinct and well-defined curves; i.e., the turbulence is bistable.

The temperature dependence of the observed critical velocities [defined as the mean positions of the discontinuous jumps; see Fig. 2(b)] is shown in Fig. 2(c). Here, a new critical velocity—type "II"—appears below 1.7 K, which coincides with the beginning of the bistable regime. In this bistable regime, as the flow velocity decreases, the intermediate turbulent state with lower dissipation (i.e., higher velocity at a given drive) destabilises, but rather than becoming laminar again, the flow transitions into the state

with stronger turbulence (i.e., lower velocity at a given drive), as can be seen in Fig. 2(b). This results in a highly unusual "backward" transition [critical velocity II in Fig. 2(b)] into a state with *higher* dissipation as the flow velocity *decreases*.

The microscopic confinement and large aspect ratio of our flow suggests the use of a 2D theory such as the Onsager vortex gas model [7,12]. However, our system deviates from the Onsager model in several important aspects: it is dissipative, continuously driven, and the confinement is large compared to the thickness of a quantized vortex ($\approx 10^{-10}$ m). Since our measurements have been conducted at relatively high temperatures, mutual friction will strongly attenuate any highly curved vortex structures. Therefore, for the sake of simplicity of the modeling, we assume that the majority of the vortices in our system can be described by two populations with definite orientations; i.e., the vortices are approximately pointlike (see Ref. [24] for more detailed analysis). We note, however, that a population of vortices without definite polarization (i.e., loops attached to a single wall) almost certainly exists in our system. In quasi-2D modeling these can be approximated as point-vortex dipoles. Furthermore, our experiment is sensitive to the total dissipation, which is an integral quantity, and hence we cannot directly determine the presence of, e.g., negative vortex temperatures, for which we would need to know the positions and signs of the vortices [38,39]. However, the spatial separation of vortices of differing signs explains the observed bistability, hysteresis, and backward transition.

To show this, we construct a model for the number of vortices in the system that captures the essential physics. A similar approach has been adapted for 2D BECs [40,41] and 3D counterflow of He II [42]. We model the time evolution (on timescales long comparable to the flow oscillation period) of positively and negatively oriented local vortex densities, n_+ and n_-, respectively, as

$$\frac{\partial n_+}{\partial t} = a n_+ + b n_- - n_+ n_- d + g_+, \tag{1}$$

$$\frac{\partial n_-}{\partial t} = a n_- + b n_+ - n_+ n_- d + g_-. \tag{2}$$

Here, the terms on the right-hand-side correspond to removal of vortices by advection ($a < 0$), creation of new vortices by splitting of seed vortices ($b > 0$), annihilation of a pair of vortices of opposite orientation ($d > 0$), and creation of vortices by large-scale shear ($g_\pm > 0$). We note in passing that these equations are similar to the Lotka-Volterra, or predator-prey, equations used to model population dynamics in ecology [43], oscillatory chemical reactions [44], or, indeed, the transition to turbulence [45]. Restricting the model to total vortex density $n = n_+ + n_-$ and polarization $s = (n_+ - n_-)/n$, we have

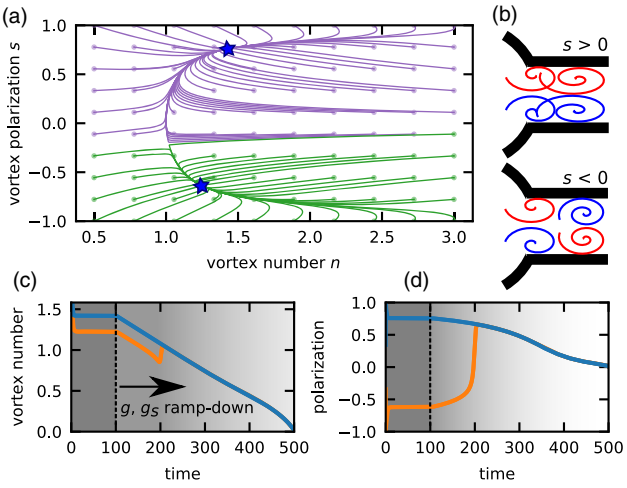

FIG. 3. Bistability of the quasi-2D model, Eqs. (3) and (4), for an example set of parameters $a = -1$, $b = 0.5$, $d = 3$, $g = 2$, and $g_s = 0.1$. (a) Starting from initial conditions indicated by the filled circles, the solution to Eqs. (3) and (4) approaches (indicated by the color of the trajectory) one of the stationary points shown as the blue stars. (b) Illustration of the two turbulent states. The large-scale polarization of the flow is either aligned ($s > 0$) or antialigned ($s < 0$) with the polarization of the drive [cf. Fig. 1(c)]. (c),(d) The backward transition in n (c) and s (d) during linear (in time) ramp-down of the generation parameters g and g_s in the range $100 < t < 500$. The flow is preferentially driven into the $s > 0$ state. For sufficiently large number of vortices n, however, $s < 0$ is also stable (i.e., the flow state can absorb oppositely oriented vortices without collapsing). As the drive—and thus the vortex number—decreases, the $s < 0$ state becomes unstable and the flow switches to the $s > 0$ state. The drive and flow are now aligned; thus the vortex number increases.

$$\frac{\partial n}{\partial t} = (a + b) n - \frac{1}{2} d n^2 (1 - s^2) + g, \tag{3}$$

$$\frac{\partial s}{\partial t} = -2bs + \frac{1}{2} d n s (1 - s^2) + \frac{g_s}{n}, \tag{4}$$

where $g = g_+ + g_-$ and $g_s = [(1 - s) g_+ - (1 + s) g_-]$, which we take as our control parameters and assume their independence of s and n (see Ref. [24] for details). The term g_s represents the polarization of the drive, i.e., the separation of generation of positive and negative vortices on the opposing corners of the channel (see Fig. 1). The vortex densities $n_\pm$ and vortex generation terms $g_\pm$ are local, whereas only the total drag, determined by the total number of vortices n, is measured in the experiment. As a first approximation we can replace the density n by its spatial average. The polarization s is antisymmetric with respect to the device axis (see Fig. 1) and its average vanishes, assuming that the flow remains neutral. Therefore we decompose $s(\mathbf{r})$ into a series of appropriate orthogonal modes $s(\mathbf{r}) = \sum_k s_k(\mathbf{r})$. Truncating the expansion after the leading term, we use Eq. (4) for calculating the evolution of

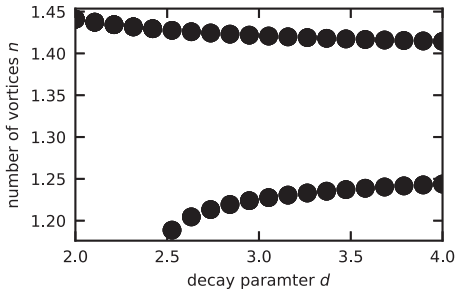

FIG. 4. The appearance of the bistable behavior controlled by d (other parameters remain unchanged). The parameter d is related to the cross section for reconnection of colliding vortices. With decreasing temperature, the vortex motion is less damped, thus making the vortices more curved. "Wiggly" vortices occupy larger area and are therefore more likely to reconnect. The appearance of the bistability with increasing d is therefore in qualitative agreement with the measured temperature dependence.

a single mode which captures the large-scale polarization of the vortex distribution.

The dynamical system of Eqs. (3) and (4) indeed has two stationary solutions for certain choices of parameters that differ in both s and n, as shown in Fig. 3(a). The essential reason for the existence of two distinct steady states of vortex number n is that $g_s \neq 0$ [i.e., the drive is polarized; see Figs. 1(c) and 3(b)], which lifts the degeneracy of $s > 0$ and $s < 0$ stationary solutions, when they exist.

By starting the evolution of the system from either of the stationary solutions and switching off the generation terms g, g_s linearly in time, we model the velocity ramp-down experiment. The result, shown in Figs. 3(c) and 3(d), reproduces the unusual backward transition observed experimentally. The transition occurs due to destabilization of the $s < 0$ polarization state, which is stabilized only at sufficiently high vortex densities n (i.e., the flow state is robust enough to withstand the oppositely polarized drive). As the drive, and the overall vortex number, decreases, this state destabilizes and transitions into the $s > 0$ state. When the flow and drive polarizations are aligned, fewer vortices are annihilated and thus the vortex density n temporarily increases.

Finally, the temperature dependence of the experimental observations can be connected, for example, with the parameter d, which is related to the cross section for reconnection of colliding vortices. This will increase with vortex deformation which, in turn, is expected to increase with decreasing temperature [46]. As shown in Fig. 4, the bistability does indeed appear as d increases, in qualitative agreement with the data.

In conclusion, using a microfluidic Helmholtz resonator we have demonstrated a long-lived bistable turbulent behavior in superfluid ^{4}He restricted to quasi-2D channel, which exists below a certain critical temperature. In addition, we observe an unusual backward transition where the flow transitions into a *more* dissipative state as the flow velocity *decreases*. The bistability, hysteresis, and the backward transition of the observed turbulence are understood in terms of a model of vortex density as an interplay between spontaneous flow ordering and polarization of turbulence generation. The proposed model is, in principle, applicable to other systems with discrete vorticity (e.g., BECs, superfluid ^{3}He) if the generation of turbulence is in some manner polarized. An interesting question is whether similar behavior is possible in continuous classical systems (indeed, random switching between two degenerate flow configurations has been observed [47]). The backward transition is of particular interest, as one usually expects turbulent fluctuations to decrease as the flow driving them is reduced. Considering that the driving mechanisms of, for example, atmospheric or oceanic flows—which are approximately 2D on large scales [2]—are typically not homogeneous and isotropic, the bistable behavior could have implications for weather prediction, climate modeling, and atmospheres of gas giants [48].

This work was supported by the University of Alberta, Faculty of Science; the Natural Sciences and Engineering Research Council, Canada (Grants No. RGPIN-04523-16, No. DAS-492947-16, and No. CREATE-495446-17); and the Canada Foundation for Innovation. We are grateful to G. G. Popowich for technical assistance and F. Souris for the velocity calibration theory.

*ev@ualberta.ca
†jdavis@ualberta.ca

[1] B. K. Arbic, K. L. Polzin, R. B. Scott, J. G. Richman, and J. F. Shriver, J. Phys. Oceanogr. **43**, 283 (2013).
[2] A. Pouquet and R. Marino, Phys. Rev. Lett. **111**, 234501 (2013).
[3] M. Rivera, P. Vorobieff, and R. E. Ecke, Phys. Rev. Lett. **81**, 1417 (1998).
[4] P. Tsai, Z. A. Daya, and S. W. Morris, Phys. Rev. Lett. **92**, 084503 (2004).
[5] U. Frisch, *Turbulence: The Legacy of A. N. Kolmogorov* (Cambridge University Press, Cambridge, England, 1995).
[6] N. Navon, C. Eigen, J. Zhang, R. Lopes, A. L. Gaunt, K. Fujimoto, M. Tsubota, R. P. Smith, and Z. Hadzibabic, Science **366**, 382 (2019).
[7] R. H. Kraichnan and D. Montgomery, Rep. Prog. Phys. **43**, 547 (1980).
[8] G. Boffetta and R. E. Ecke, Annu. Rev. Fluid Mech. **44**, 427 (2012).
[9] G. Gauthier, M. T. Reeves, X. Yu, A. S. Bradley, M. A. Baker, T. A. Bell, H. Rubinsztein-Dunlop, M. J. Davis, and T. W. Neely, Science **364**, 1264 (2019).
[10] S. P. Johnstone, A. J. Groszek, P. T. Starkey, C. J. Billington, T. P. Simula, and K. Helmerson, Science **364**, 1267 (2019).
[11] Y. P. Sachkou, C. G. Baker, G. I. Harris, O. R. Stockdale, S. Forstner, M. T. Reeves, X. He, D. L. McAuslan, A. S. Bradley, M. J. Davis, and W. P. Bowen, Science **366**, 1480 (2019).

[12] L. Onsager, Nuovo Cimento **6**, 279 (1949).
[13] M. T. Reeves, T. P. Billam, X. Yu, and A. S. Bradley, Phys. Rev. Lett. **119**, 184502 (2017).
[14] M. T. Reeves, T. P. Billam, B. P. Anderson, and A. S. Bradley, Phys. Rev. Lett. **110**, 104501 (2013).
[15] D. R. Tilley and J. Tilley, *Superfluidity and Superconductivity*, 3rd ed. (Institute of Physics Publishing, Bristol, 1990).
[16] C. F. Barenghi, L. Skrbek, and K. R Sreenivasan, Proc. Natl. Acad. Sci. U.S.A. **111**, 4647 (2014).
[17] P. Walmsley, D. Zmeev, F. Pakpour, and A. Golov, Proc. Natl. Acad. Sci. U.S.A. **111**, 4691 (2014).
[18] E. Fonda, K. R. Sreenivasan, and D. P. Lathrop, Proc. Natl. Acad. Sci. U.S.A. **116**, 1924 (2019).
[19] A. W. Baggaley, C. F. Barenghi, and Y. A. Sergeev, Phys. Rev. E **89**, 013002 (2014).
[20] X. Rojas and J. P. Davis, Phys. Rev. B **91**, 024503 (2015).
[21] F. Souris, X. Rojas, P. H. Kim, and J. P. Davis, Phys. Rev. Applied **7**, 044008 (2017).
[22] A. J. Shook, V. Vadakkumbatt, P. Senarath Yapa, C. Doolin, R. Boyack, P. H. Kim, G. G. Popowich, F. Souris, H. Christani, J. Maciejko, and J. P. Davis, Phys. Rev. Lett. **124**, 015301 (2020).
[23] S. Forstner, Y. Sachkou, M. Woolley, G. I. Harris, X. He, W. P. Bowen, and C. G. Baker, New J. Phys. **21**, 053029 (2019).
[24] See Supplemental Material at http://link.aps.org/supplemental/10.1103/PhysRevLett.125.025301 for details on experimental setup, pressure gradient and velocity calibration, discussion on two dimensionality, further analysis and extension of the theoretical model, and additional data, which includes Refs. [25–36].
[25] H. A. Kierstead, J. Low Temp. Phys. **23**, 791 (1976).
[26] D. J. Bishop and J. D. Reppy, Phys. Rev. Lett. **40**, 1727 (1978).
[27] S. Jose Benavides and A. Alexakis, J. Fluid Mech. **822**, 364 (2017).
[28] S. Babuin, E. Varga, L. Skrbek, E. Lévêque, and P.-E. Roche, EPL **106**, 24006 (2014).
[29] M. T. Reeves, T. P. Billam, B. P. Anderson, and A. S. Bradley, Phys. Rev. Lett. **114**, 155302 (2015).
[30] A. Pouquet, R. Marino, P. D. Mininni, and D. Rosenberg, Phys. Fluids **29**, 111108 (2017).
[31] A. Duh, A. Suhel, B. D. Hauer, R. Saeedi, P. H. Kim, T. S. Biswas, and J. P. Davis, J. Low Temp. Phys. **168**, 31 (2012).
[32] K. W. Schwarz, Phys. Rev. B **31**, 5782 (1985).
[33] R. J. Donnelly, *Quantized Vortices in Helium II* (Cambridge University Press, Cambridge, England, 1991).
[34] R. J. Donnelly and C. F. Barenghi, J. Phys. Chem. Ref. Data **27**, 1217 (1998).
[35] G. W. Stagg, N. G. Parker, and C. F. Barenghi, Phys. Rev. Lett. **118**, 135301 (2017).
[36] E. J. Hopfinger, F. K. Browand, and Y. Gagne, J. Fluid Mech. **125**, 505 (1982).
[37] J. Gao, W. Guo, S. Yui, M. Tsubota, and W. F. Vinen, Phys. Rev. B **97**, 184518 (2018).
[38] A. J. Groszek, M. J. Davis, D. M. Paganin, K. Helmerson, and T. P. Simula, Phys. Rev. Lett. **120**, 034504 (2018).
[39] R. N. Valani, A. J. Groszek, and T. P. Simula, New J. Phys. **20**, 053038 (2018).
[40] A. J. Groszek, T. P. Simula, D. M. Paganin, and K. Helmerson, Phys. Rev. A **93**, 043614 (2016).
[41] A. Cidrim, F. E. A. dos Santos, L. Galantucci, V. S. Bagnato, and C. F. Barenghi, Phys. Rev. A **93**, 033651 (2016).
[42] E. Varga and L. Skrbek, Phys. Rev. B **97**, 064507 (2018).
[43] A. A. Berryman, Ecology **73**, 1530 (1992).
[44] A. J. Lotka, J. Phys. Chem. **14**, 271 (1910).
[45] H. Y. Shih, T. L. Hsieh, and N. Goldenfeld, Nat. Phys. **12**, 245 (2016).
[46] C. F. Barenghi, R. J. Donnelly, and W. F. Vinen, Phys. Fluids **28**, 498 (1985).
[47] M. L. Woyciekoski, L. A. M. Endres, A. V. de Paula, and S. V. Möller, Ocean Eng. **195**, 106658 (2020).
[48] R. M. B. Young and P. L. Read, Nat. Phys. **13**, 1135 (2017).